

https://doi.org/10.1093/pnasnexus/pgaf314 Advance access publication 16 October 2025 Research Report

Conservation of glial density and cell-type ratios within a brain region across mammals

Antonio Pinto-Duarte^{a,b}, Katharine Bogue o, Terrence J. Sejnowski and Shyam Srinivasan and Shyam Srinivasan

Edited By Andrey Abramov

Abstract

Glial cells in the brain are as numerous as neurons, but their organization is less understood. One view suggests that glial organization is similar across brain regions. To better understand glial organization, we examined functionally and architecturally diverse neural circuits in humans, other primates, carnivores, and rodents using histology and single nucleus RNA sequencing datasets. We focused on microglia, oligodendrocytes, and astrocytes, which constitute the major glial cell types. Across mammals, while glial volume densities and proportions of glial cell types are preserved within a region, they vary across regions in the brain, suggesting that glial organization is not uniform but circuit-dependent. Additionally, the ratio of glia to neurons increases with brain volume according to a ¹/₄ power law in the primate frontal cortex, the neocortex, the piriform cortex, and the cerebellum. These findings show that glial and neuronal development and function are tightly coupled, and a circuit's function depends as much on its glia as its neurons.

Keywords: brain scaling, glial organization, primates, evolution, glia-neuron ratios

Significance Statement

While many studies focus on neurons in cognition, fewer examine glia, which are crucial for memory, plasticity, circuit communication, and brain health. Consequently, principles of glial organization are less understood. We present a framework for glial organization in mammals, where each brain region has unique, conserved glial densities and compositions that distinguish it from other regions. Additionally, glia-to-neuron ratios scale consistently across species and circuits, revealing a tight coupling between glia and neurons. These organizational features, observed across mammals including humans and other primates, highlight their central role in a circuit's architecture and their importance in understanding cognition and brain health.

Introduction

Numerous studies have examined how neuronal components in brain circuits scale with brain size (1–5), a strategy that has improved our understanding of circuit design by linking architecture, information coding, and function (4, 6, 7). Neurons, however, are only half the story, with brains containing just as many glial cells (8). A similar in-depth quantitative examination of glial features, however, is limited to a few species or gross brain structures, e.g. the neocortex (9, 10). Quantifying features of glial organization across brain areas and species is a critical step in identifying patterns of correlated glial and neural features and generating hypotheses about why and how these features are related. Here, organization refers to the spatial distribution of glial cells, which can be inferred from measurements of cell densities and relative

ratios—either between glial cell types or between glial and neuronal cells.

Like neurons, glia are morphologically and functionally distinguishable into several types (11). The three major types include astrocytes, which are involved in critical functions such as synaptic transmission and plasticity, synchronization of neural networks, and energy metabolism (12–16); microglia, which play a key role in local immune responses through phagocytosis (17); and oligodendrocytes, which enhance neuronal communication by providing axon myelination (11, 18, 19). Previous studies have aggregated these distinct cell types when examining gross brain regions like the neocortex (9, 20). As a first step, the studies have been insightful, such as Sherwood et al. (10) showing that glia-to-neuron ratios or GNRs increase with bigger brains in the prefrontal cortex in primates. Bigger brains have greater neuronal (and network)



Competing Interest: The authors declare no competing interests.

Received: September 9, 2024. Accepted: September 8, 2025

^aComputational Neurobiology Laboratory, Salk Institute for Biological Studies, 10010 North Torrey Pines Road, La Jolla, CA 92037, USA

^bInstitute for Neural Computation, University of California San Diego, 9500 Gilman Drive, San Diego, CA 92093, USA

^cMolecular Neurobiology Laboratory, Salk Institute for Biological Studies, 10010 North Torrey Pines Road, La Jolla, CA 92037, USA

^dDepartment of Neurobiology, University of California San Diego, 9500 Gilman Drive, San Diego, CA 92093, USA

^{*}To whom correspondence should be addressed: Email: shyams@uci.edu

complexity and energy demands, and a greater number of glia predicted by GNR scaling laws helps meet this demand.

To understand glial systems better, we need to build on such studies by advancing to the next step of understanding how individual glial cell types vary across circuits and species. Current evidence suggests that glial compositions, i.e. the proportions of different glial cell types, are similar across circuits (21). But, neural circuits vary by the functions they perform and this is reflected in their connectivity and neuronal cell composition (4, 7, 22). If neuronal organization is unique to a circuit, and glial cells support neuronal function, shouldn't they also be unique? And shouldn't glial features be conserved within conserved circuits within the same circuit across species?

We can test these hypotheses by quantifying glial compositions across circuits and species in two complementary ways. First, we can directly count each glial cell type within circuits and compare them (and compositions) across circuits and species to determine if glial organization is conserved within circuits but varies between them. Second, when direct cell-type counts are not feasible, we can use glial cell densities as a proxy for composition. Additionally, if glial densities are preserved within circuits but neuronal densities change predictably across species, then GNRs should reveal systematic scaling relationships between glial and neuronal organization across brain sizes.

To test these predictions across diverse neural architectures, we chose to examine four circuits that represent a measure of diversity present in brain circuits. Circuits can be distinguished on the basis of their (i) connectivity—topographic (there is a map or connections are predictable, e.g. the visual circuit where nearby neurons in the retina connect to nearby neurons in V1) or distributed (connections are unpredictable, e.g. connections from the olfactory bulb (OB) to piriform cortex (PCx)), (ii) lamination—number of layers, (iii) function—the kind of information that is processed, and (iv) circuit size in neuron numbers. Based on these factors, we examined the anterior piriform cortex or APCx, posterior piriform cortex or PPCx, the entorhinal cortex or ECx, and the cerebellum across species. These regions are significantly distinct from the well characterized neocortex, and each other. The cerebellum contains 70% of the neurons in the human brain (23–25) and has a unique type of "specialized" radial astrocytes: the Bergmann glia. The anterior and posterior piriform cortices (Fig. 1a) are both trilaminar structures with distributed connectivity (26). Finally, the entorhinal cortex (ECx) is a multimodal circuit that mixes sensory information from topographic and distributed circuits for higher cognitive tasks such as spatial navigation (27, 28). Importantly, our study covered a range of species including humans, other primates, carnivores, and rodents. We used diverse methods including histology, transgenic mice, and analyses of single nucleus RNA sequencing (snRNAseq) datasets.

We found three key glial organizational properties across diverse circuits and species. First, glial densities remain constant within a circuit across species while varying between circuits. Second, glial cell compositions, too, are conserved within circuits but differ between them, suggesting that individual glial cell types play consistent roles within each circuit across species. Third, GNRs increase with brain size at similar rates across different circuits, implying strong coupling between neurons and glia. Thus, each circuit has a unique glial organization, which evolution has maintained across species.

Materials and methods

In this study, we conducted experiments to measure the number of glia in PCx and ECx in Mus musculus (mouse), Rattus novergicus (rat), Cavia porcellus (guinea pig), Mustela putoris furo (ferret), Monodelphis domestica (short-tailed opossum), Felis catus (domestic cat), Macaca mulatta (rhesus macaque), Callithrix jacchus (marmoset), and Homo sapiens (humans) using Nissl (Figs. 1 and 2), immunofluorescence (IF, Figs. 1 and 5), and immunohistochemistry (IHC, Figs. 1, 2, and 5). Animal care protocols were approved by the Salk Institute Animal and Use Committee and conform to US Department of Agriculture regulations and National Institutes of Health guidelines for humane care and use of laboratory animals. Below, we provide a brief description of the methods we used for staining, obtaining cellular and volumetric estimates of each circuit, and the analysis done on single cell sequencing datasets. For detailed descriptions, please refer to Supplementary methods.

Histology and staining

Here, we used similar procedures to earlier studies (7, 9, 29) to perform histology. We describe them briefly here and in more detail in Supplementary methods. To validate the use of Nissl stains, we took advantage of available human, marmoset, and mouse tissue to examine counts of individual glial-types using DAB (DAB, 3,3'-diaminobenzidine) staining (Figs. 2 and 6) as previously done (30) and immunofluorescence (IF) staining, and compared them with counts obtained on tissue that were Nissl stained. We could not extend DAB or IF staining to other species due to lack of available tissue, and used Nissl stains, instead. In this regard, the use of Nissl stains with stereological methods, combining light microscopy and morphological criteria, are still among the most efficient, especially when it is necessary to differentiate and count large quantities of glia and neurons across the layers of different brain regions and the brains of multiple species.

Stereology and volumetric estimates

We used stereology and volumetric estimates to estimate the density of glia and individual glial cell-types across layers of the anterior piriform cortex (APCx), the posterior piriform cortex (PPCx), and entorhinal cortex (ECx) with the help of Neurolucida (version 10.53; MBF Bioscience, Wilmington, VA, USA) at low magnification (2x and 4x objectives) based on standard atlases and primary literature (26, 31–34). To estimate cell number we examined 10 or $20 \,\mu\text{m}$ -wide columns, perpendicular to the pial surface, extending down to the boundary of the deepest layer, which we delineated with the Neurolucida contours option. The sections and columns within them were chosen so that we had equal coverage of the region along the rostral-caudal and dorsal-ventral axes. For obtaining surface area density counts (number of glia/ mm²), three measures were used: the width of the column, the thickness of the section, and the number of neurons in the column. Columns were randomly chosen while ensuring that they were close to perpendicular to our coronal cut and the surface of the brain (as an illustration, Table S6 shows the number of columns in each species for APCx). We used the same procedure for Nissl, IF, DAB staining, and Sox9-EGFP mice.

Statistical analysis

We performed two types of statistical analyses. First were analyses for significance of the results we reported in Figs 3, 4, 5, 6, S2, S3, and S4. We computed the R2 and Pearson's correlation coefficient using the R statistical programming language, and listed them in the figures and the results section of the main text. Second, we performed analyses on transcriptomic datasets across several brain regions in primates from (36-38). Briefly, Fig. 7a contains an analysis of the dataset from (36) who examined cell types in the middle temporal gyrus or MTG of five primates: gorilla, chimpanzee,

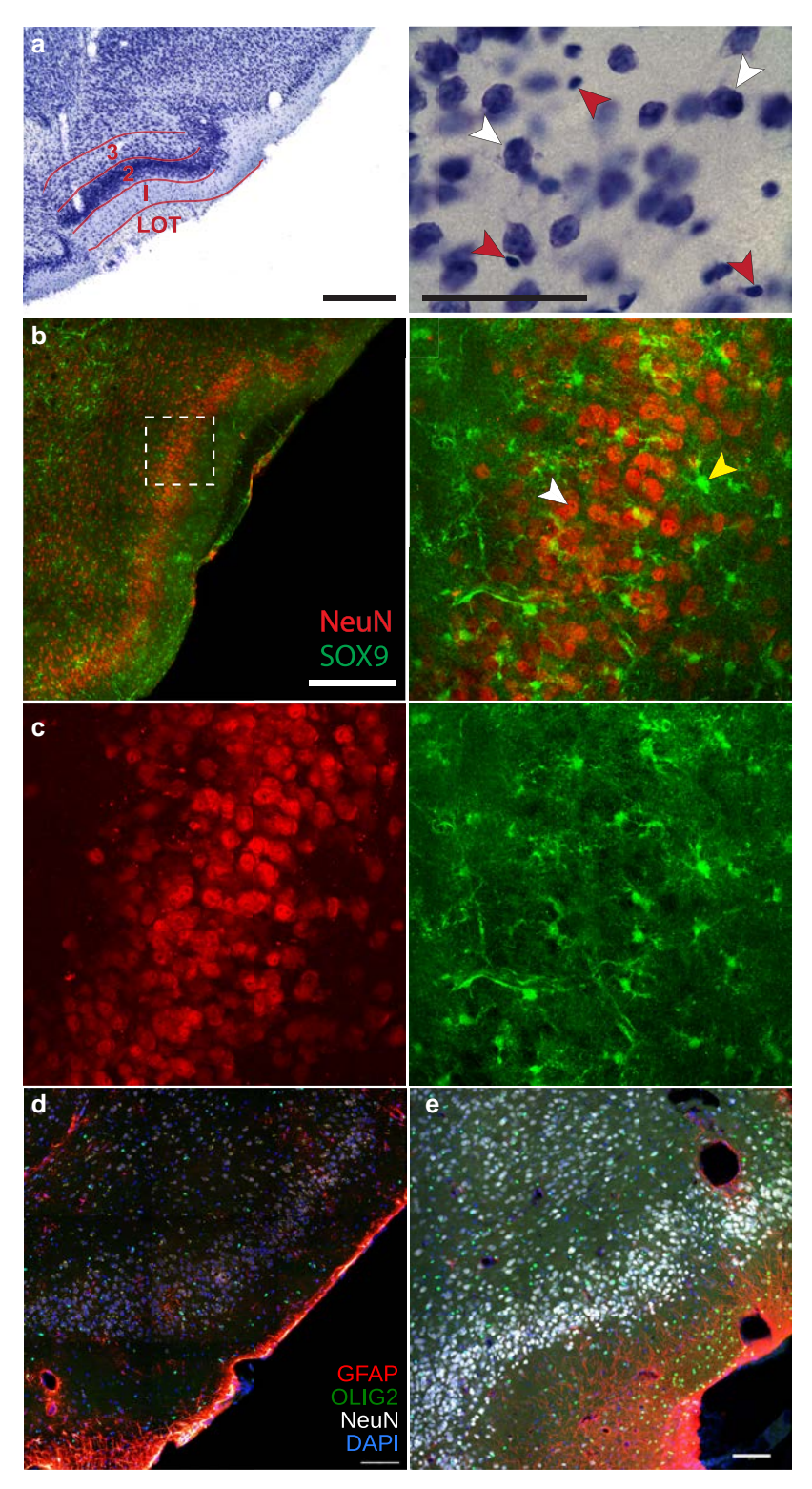


Fig. 1. Identification of neurons, glia, astrocytes, and oligodendrocytes in histological sections of the APCx. a, left panel) Nissl-stained coronal section in a mouse showing the three layered piriform cortex. Layer 2 is readily identifiable because of the extremely high density of neurons; layer 1 is cell-scarce, and layer 3 has intermediate cell density. Scale bar: 500 µm. a, right panel) Magnified image of (a, 2x magnification) at a 100x magnification showing neurons and glia in layer 3. Neurons (two white arrowheads) are distinguishable from glia (three red arrowheads) by their larger size and morphology (glia appear smaller and are more punctate, see Supplementary methods for detailed descriptions). b, left panel) Example of a section of the APCx of Sox9-EGFP mice co-labeled with the neuron marker, NeuN. Astrocytes and neurons are false-colored in green and red, respectively. The density of NeuN labeled cells clearly distinguishes layer 2 from the other layers. Scale bar: 200 µm. Inset dotted line square (edge length: 200 µm) is shown on the right panel with arrow heads marking neurons (left arrowhead) and astrocytes (right arrowhead). c) The left and right panels show the same image as (b, right panel) with only neurons (marked in red, left) or glia (marked in green, right). d, e) A coronal section through mouse (d) and marmoset (e) APCx labeled for Astrocytes (GFAP, red), Oligodendrocytes (OLIG2, green), Neurons (NeuN, white), and DAPI. See Figs. S7 and 6 for a magnified view of mouse and marmoset APCx, respectively. Astrocytes are discernible by the processes surrounding the soma which has a purple/pink color from colabeling by GFAP and DAPI, and oligodendrocytes are discernible by a bluish green color from colabeling by OLIG2 and DAPI (Figs. 2c, S7a, and S9c). Scale bar is 100 µm. APCx, anterior piriform.

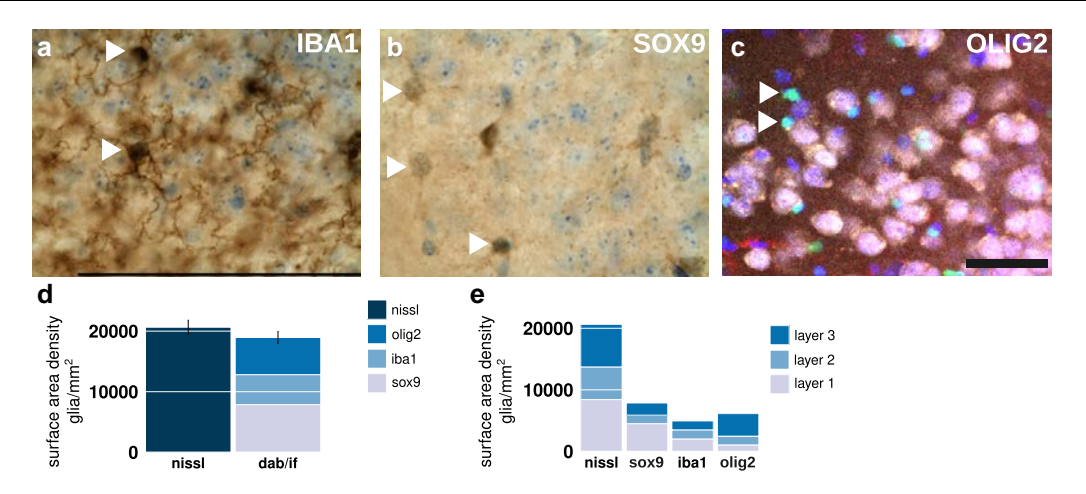


Fig. 2. Glia in the anterior piriform cortex of mice. a-c) high magnification images of the anterior piriform cortex in a mouse stained with DAB or IF for marking astrocytes, microglia, and oligodendrocytes. In (a, b), the glial cell types can be distinguished (marked by arrows) by cells co-stained with DAB in brown and Nissl in blue. In c), oligodendrocytes are marked by co-staining of OLIG2 in green and DAPI in blue. a) Microglia marked for IBA1. b) Astrocytes marked for SOX9. c) Oligodendrocytes marked for OLIG2. White arrowheads highlight glial cell types co-stained with DAB and Nissl, and IF. d, e) Estimates of number of cells under a mm2 of anterior piriform cortex using DAB and Nissl, and IF staining. d) Shows the estimates of the total number of glial cell types measured with DAB and Nissl, and IF stains. The dab/if staining bar on the right is broken into three sections, each section a different color denoting the three major glial cell types: sox9 in gray for astrocytes (bottommost), iba1 in light blue for microglia (middle), and olig2 in dark blue (with IF, top). The bar on the left denotes the estimate of total number of glia under a mm2 of surface measured in Nissl stains. The error bars are SEM, for an n of 2 for both estimates, and the dab/if staining SEM is calculated by error propagation assuming independence between DAB and IF staining. e) Shows overall glia and each glial cell type distribution across layers. The nissl bar shows the total number of glia in every layer, and the other three show the individual distribution of each glia-type in every layer. Scale bar: 100 µm for a and b, and 25 µm for (c). See Fig. S4 for the distribution of glial-cell types in each layer. Protein marker names (sox9, olig2) and histological stains (nissl, dab) in data plots are shown in lowercase as a visual convention for quantitative measurements of positive cells or stained areas. DAB, 3,3'-diaminobenzidine; IF, immunofluorescence; SEM, standard error of the mean.

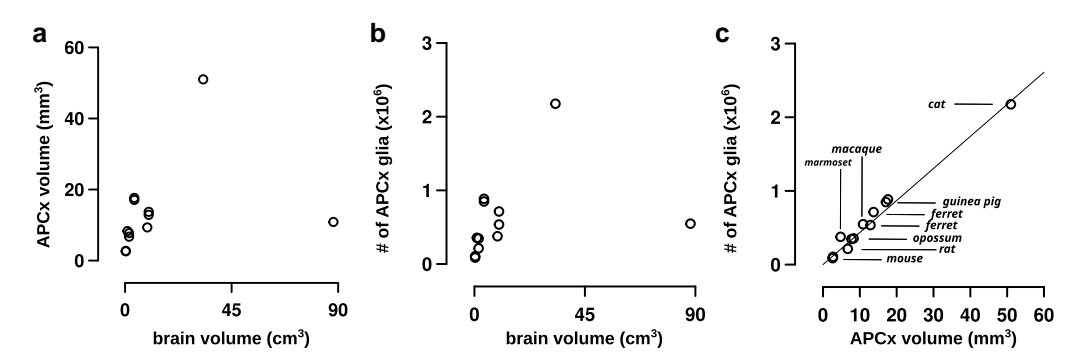


Fig. 3. Glial volume densities were constant across species in APCx The APCx volume (a) and number of glia contained in it (b) increase with brain volume. c) Despite significant differences in APCx volume and absolute number of glia across the different species studied, the number of glia per mm³ was approximately the same, being an excellent fit for the equation, y = 43,500x with an R2 of 0.98 (95% CI: 39,890-48,090 glia/mm3). See also Tables S1 and S2 for the numerical values plotted in the graphs. APCx, anterior piriform cortex.

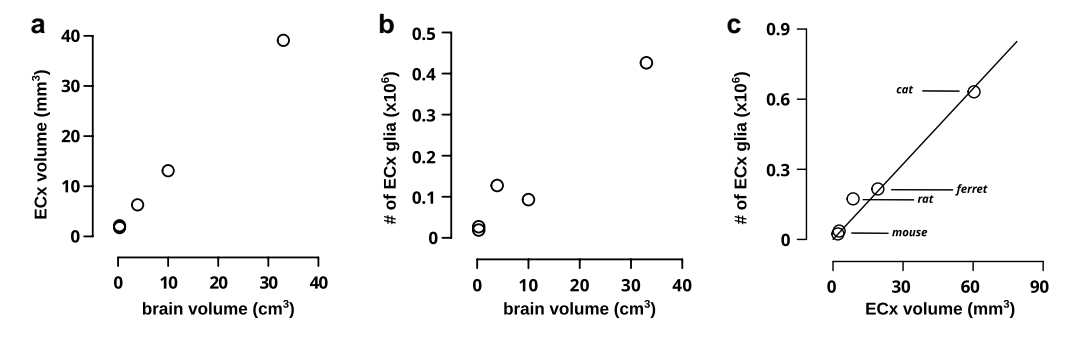
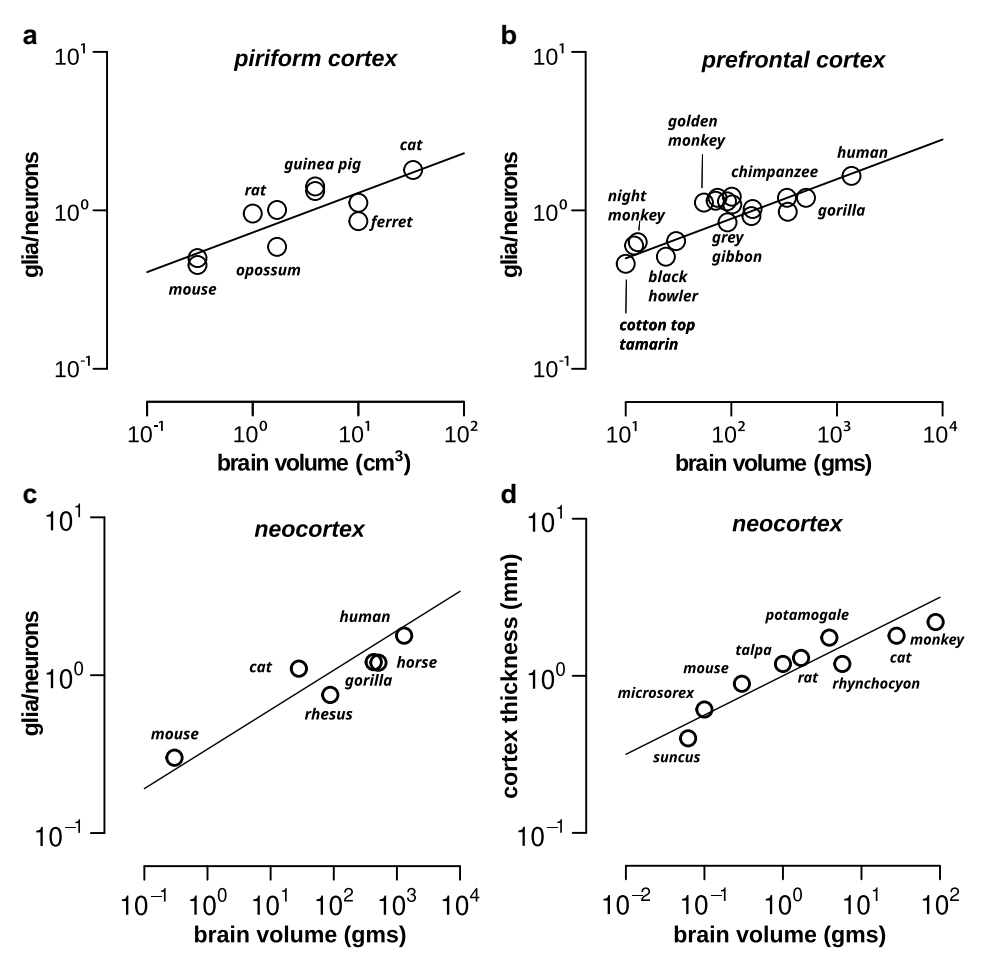


Fig. 4. Glial volume densities were constant across species in ECx. The ECx volume (a) and number of glia contained in it (b) increased with brain volume across the species studied. c) The number of glia per mm³ was approximately the same in the ECx across the species studied, and was fitted with a line represented by the equation y = 11,000x with an R² of 0.97 (95% CI: 7,490-12,570 glia/mm³). See also Tables S1 and S2 for the numerical values plotted in the graphs, and Fig. S4d for a comparison of densities between regions. ECx, entorhinal cortex; CI, confidence interval.



 $\textbf{Fig. 5.} \hspace{0.2cm} \textbf{Glia-neuron ratio increases with the size of the brain. a) GNR in APCx of six mammals shows that in APCx, GNR increases with brain size as <math>y=0.72x^{1/4}$ (R2 = 0.67, 95% CI: 0.1-0.38). Note that most species have multiple animals that were examined. For number of glia, see Table S1, and for number of neurons see Table S3 of Ref. 7). b) GNR replotted from (10) showing that as the size of the primate brain increases, GNRs in PFC increase. The numerical values were fitted with a line according to the equation $y = 0.3x^{1/4}$ ($R^2 = 0.68$, 95% CI: 0.14–0.29), c) GNR in the neocortex as a whole measured in six mammals shows that as brain volume increases across species, so does the ratio of glia to neurons. The data are fit to a power-law equation $y = 0.34x^{1/4}$ ($R^2 = 0.88, 95\%$ CI: 0.05–0.3). d) The thickness of the cortex increases with brain size, represented here with weight. The data include five insectivores (35) and four mammals (9). The fitted line has the equation, $y = x^{1/4}$, ($R^2 = 0.86$, 95% CI: 0.13–0.28). GNR, glia to neuron ratio; APCx, anterior piriform cortex; PFC, prefrontal cortex; CI, confidence interval.

marmosets, macaques, and humans. Figure 7b contains an analysis of datasets from (37, 38), who examined cell types through snRNA-seq in rhesus macaques and marmosets, respectively.

Results

Our goal with this study was to test if glial measures such as densities, cell-type compositions, and number of glia relative to neurons can be expressed by simple scaling laws in diverse brain regions in mammals. A note on densities: We measured two kinds of densities, surface area densities that give the number of cells under a mm² of pial surface, and volume densities that give the number of cells per mm³. We explicitly mention which density we measured. By default, density refers to volume densities. First, we wanted to investigate if glial measurements obtained with Nissl and other types of staining yielded comparable results and could be used interchangeably.

Estimates of glia in anterior piriform cortex with Nissl, IHC and IF staining are similar

We began by seeking to ascertain if glia count estimates using Nissl stains are accurate, since we only had Nissl-stained tissue for all species analyzed. To do so, we used multiple methods to

estimate the number of glia in mouse anterior piriform cortex: Nissl, IHC or DAB, and IF staining. Additionally, we used endogenously expressed Sox9 to estimate astrocytes. Figure 1 shows representative coronal sections (humans in Fig. 6).

First, we labeled three types of glia—astrocytes, microglia, and oligodendrocytes—simultaneously with Nissl and DAB staining, as done previously (30). We marked astrocytes by staining for SOX9 using DAB, and then co-stained for Nissl (using Thionin). We manually counted astrocytes by identifying cells with simultaneous expression of DAB and Nissl (Fig. 2b). We repeated this procedure for microglia (marked for IBA1, Fig. 2a), and oligodendrocytes (marked for OLIG2, Fig. S9a).

Second, we used IF (see Materials and methods) to estimate astrocyte and oligodendrocyte numbers. As shown in Figs. 1d, 2c, S7a, and S9c, we marked oligodendrocytes using OLIG2 in green, astrocytes using GFAP in red, neurons using NeuN in white with DAPI counterstaining of nuclei in blue. We found neuron surface area densities for the two mice to be 58,101 and 63,000 neurons/mm² agreeing with the published estimate of 58,753 neurons/mm² (29), and providing a validation point for the staining and counting procedures.

The estimates of glia by Nissl, DAB, and IF staining were comparable (Figs. 2d and S7). We compare surface area densities of overall glia obtained with Nissl stains (in dark blue) with

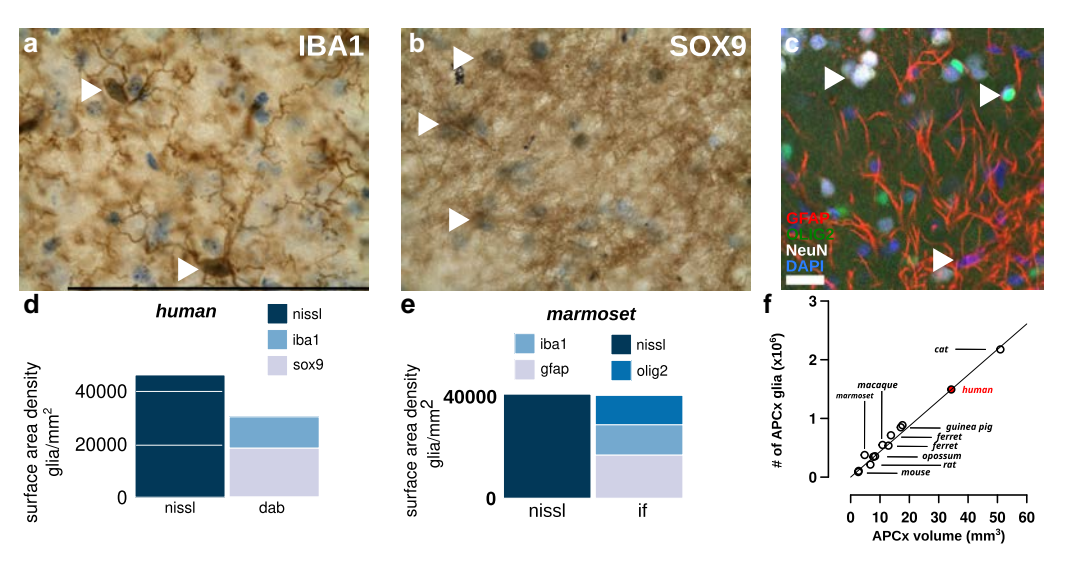


Fig. 6. Glia in the anterior piriform cortex of humans. a, b) High magnification images of the anterior piriform cortex (PCx) in a human stained with DAB for marking astrocytes and microglia. In each image, the glial cell types can be distinguished (marked by arrows) by cells stained with DAB in brown, co-stained with Nissl in blue. a) Microglia marked for IBA1. b) Astrocytes marked for SOX9. c) A magnified image of a section of the marmoset APCx shown in Fig. 1e. The arrowheads highlight the cells that were measured: oligodendrocytes in bluish green, astrocytes with a pink/purple soma and surrounding processes in red, and neurons in white. Scale bar is 10 µm. Cells without these characteristics were not counted. d) Shows the estimates of the total number of glial cell types measured with DAB and Nissl stains. The dab staining bar on the right is divided into two sections, each section a different color denoting sox9 in gray (bottom bar), and iba1 in light blue (top bar). The bar on the left denotes the estimate of total number of glia under a mm2 of surface measured in Nissl stains. e) Comparison of surface area densities in the marmoset with Nissl stains (left bar) and IF stains (right bar). The IF stains comprise counts from individual glial cell-types with the bottommost bluish grey bar signifying astrocytes, middle light blue bar signifying microglia, and top darker blue bar signifying oligodendrocytes. The microglia numbers here were taken from human DAB staining data on the assumption that primates might have similar microglial compositions based on cortical data (Fig. 7 and (36)). f) Replotting the scaling of APCx volume versus number of glia shown in Fig. 3c, with human data. The human data point (in red) falls on the regression line with slope 43,000 showing that evolution has preserved glial population densities across species. Scale bar: 100 µm. DAB, 3,3'-diaminobenzidine; IF, immunofluorescence.

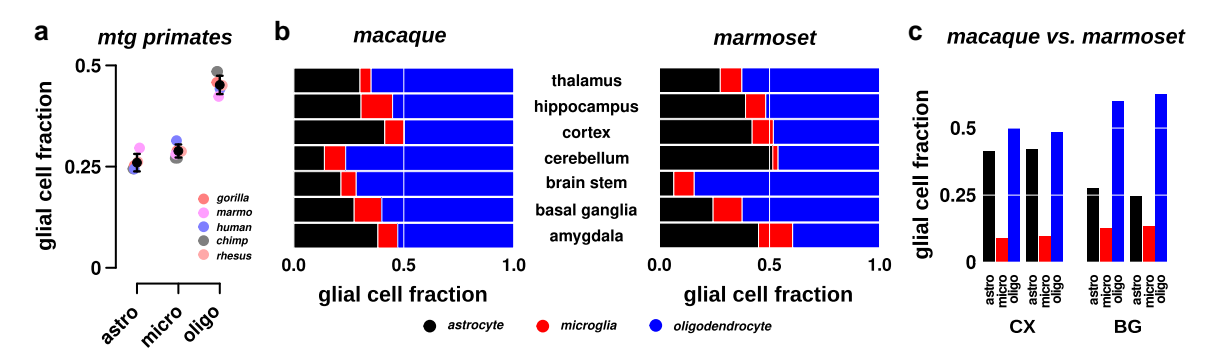


Fig. 7. Single nucleus RNA sequencing experiments across primates show glial cells to be a region specific marker. a) Comparison of glial cell compositions across the middle temporal gyrus (MTG) of gorillas, marmosets, humans, chimpanzees, and rhesus macaques shows that the proportions of each cell type (astrocytes, microglia, or oligodendrocytes) is preserved across species. See Fig. S6 for relative fractions with more nonneuronal cells endothelial cells—as well as a breakup of oligodendrocytes into oligodendrocytes and oligodendrocyte precursor cells. b) Shows the proportions of astrocytes (black, left), microglia (red, middle), and oligodendrocytes (blue, right) in seven different brain regions. On the left are results of analyzing snRNA-seq data in macaques (37) and on the right are similar studies in marmosets (38). Both show that the combination of cell proportions differ by brain region. For instance, if you compare the basal ganglia with the cortex, the basal ganglia have a smaller fraction of astrocytes, but a greater proportion of microglia. These data are also plotted in (c). See Fig. S6 for more regions and cell-types being compared. c) An example plot comparing the glial cell compositions in two different brain regions in marmosets and macaques. Visual inspection shows that the cell composition is similar in both species, in addition to showing that the cortex and basal ganglia differ in their glial cell composition. See Fig. S6 for similar comparisons of five other regions. BG, basal ganglia; CX, cortex.

individual glial cell types (gray—astrocytes, light blue—microglia, medium blue—oligodendrocytes) in Fig. 2d. In Fig. 2e, we show the breakdown of surface area densities of all glia and individual glial cell types by layer. Note that in Fig. 2 we used DAB stains for astrocytes and microglia but IF stains for oligodendrocytes, as IF staining provided more accurate counts than the lighter DAB staining for oligodendrocytes.

Examining DAB vs. IF more closely for oligodendrocytes, we found that most of the difference was attributable to layer 3 (compare layer 3 counts for the two in Fig. S7d), suggesting that DAB estimates of layer 3 oligodendrocytes might be an underestimate. In contrast, astrocytes surface area density with IF (GFAP) was not significantly different from DAB (SOX9, Fig. S7b). Thus, individual glial cell type counts match well with the overall count of glia (Figs. 1 and S7b).

For astrocytes, we used DAB staining with SOX9 (a nuclear marker (39)), and IF staining with GFAP (a marker of soma and some of the major processes) to mark different aspects of the cell (39, 40). The GFAP staining is lighter in gray matter versus

white matter or reactive astrocytes (41), creating heterogeneous labeling that was helpful for observing interlaminar astrocytes found closer to the pia (42). These interlaminar astrocytes were visible with the more extensive GFAP labeling in PCx of marmosets and humans, but not mice (Figs. 1e, 6c, and S7g,h).

We independently validated DAB and IF staining estimates of astrocytes in mice by examining the number of astrocytes using a Sox9-EGFP mouse, in which astrocytes were specifically labeled with GFP (39). As described in the Supplementary methods section, Fig. 1 shows coronal sections through the piriform cortex, with GFP-positive cells (from Sox9-EGFP mice) marked in green, and NeuN-positive cells (denoting neurons) marked in red. Figure S1 shows two comparisons. First, it shows the comparison between astrocytes and neurons across the three layers with layer 1 having the highest number of astrocytes (Fig. S1a). Second, it highlights the similarities in astrocyte/neuron ratios obtained with either Sox9-EGFP reporter expression or DAB staining (Fig. S1b), suggesting that DAB staining is effective in estimating astrocyte number.

We show later for marmosets that the proportion of astrocyte and oligodendrocyte cells captured by IF and DAB stains is similar (Figs. 6e and S7e). This consistency demonstrates that DAB and IF staining capture the proportions of glial cell types and match the cumulative glial numbers with Nissl staining. The finding gave us confidence that Nissl stains can be used to estimate glia densities across species, and we present these estimates in the next sections.

Having independently validated astrocyte and glial number estimates through multiple methods, we examined the distribution of glia across layers. Layer 1 contained most of the glia, followed by layer 3. Layer 2, which is particularly neuron-rich (Figs. 1a, b and S5a), contained the fewest glia. We then examined the composition of glia across layers starting with astrocytes. Astrocytes are important for synaptic physiology, transmission and plasticity (11, 43, 44). The higher numbers of synapses in layers 1 and 3 compared to layer 2 (26) suggests that we should observe more astrocytes in layers 1 and 3. When we examined astrocytes, this was, indeed, the case (Fig. 2e). Microglia showed a trend similar to astrocytes with most of them located in layer 1, followed by layers 3 and 2 (Fig. 2e). Oligodendrocytes, however, deviated from this trend, being highest in layer 3. The distribution of oligodendrocytes mirrored that of SMI-99 and NF-160 (Fig. S8b), two proteins that label axon filaments and myelin, which are produced by oligodendrocytes.

Notably, astrocytes were the biggest proportion of glial cell types in layer 1, which contained most of the glia, and thus, astrocytes were the most prevalent glial cell type. Overall, these features of glia distribution (Figs. 2e and S5b) might reflect the computational processes carried out in each layer (45, 46). Having validated our methods, we next use these methods to examine conserved trends of glial organization.

The volume density of glia is conserved in both parts of the piriform cortex across brain sizes

A previous study (9) showed that glial volume densities are conserved in the motor, somatosensory, parietal, and temporal regions of the neocortex of four mammals (21,100 glia/mm³) supporting even earlier findings (35) of constant glial volume densities in the neocortex of five insectivore species (Fig. S2, 25,600 glia/mm³, CI: 24,000-27,200). To test if glial volume densities are conserved within other brain regions across species, we examined the anterior piriform cortex (APCx) and posterior piriform cortex (PPCx).

We estimated the total number of glia in APCx of nine mammals including humans, other primates, carnivores, and rodents (Fig. 3, humans in Fig. 6f) and determined how they varied with APCx size, measured in terms of volume and surface area (Fig. 3a-c). Please see the volume measurement section in Supplementary methods on how we calculated a region's volume and area from reconstructions of coronal sections. We found that the number of glia increased proportionally with APCx volume (Fig. 3c, Fig. S2f for log scale). The relationship fit the equation $N_G = m*V_{APCx}$ well $(R^2 = 0.98, N_G = number of glia, V_{APCx} = volume of APCx), where$ the slope $m = N_G/V_{APCx}$ represents glial volume density (q_{vd}) : 43,500 glia/mm³ (95% CI: 39,890–48,090 glia/mm³). Glial cell number was also proportional to APCx surface area (Fig. S2) as APCx thickness varied little with size for most species (Table S4).

To validate our calculations, we used additional ways of measuring volume densities. First, we estimated glial volume density by measuring the surface area density of glia (Fig. S2b, see Tables S1 and S3 for individual animal counts), and the thickness of the APCx (Fig. S2c, see Tables S1 and S3 for individual animal counts), similar to earlier studies (9). Surface area density and thickness are related by the equation $g_{\text{sad}} = N_0 + m * T_{\text{APCx}}$, where g_{sad} is the surface area density in glia/mm², N_0 is an additive constant (intercept) in units of glia/mm², T_{APCx} is the thickness of APCx, and m is the slope in units of glia/mm³ (glial volume density). The data fit this equation well (Fig. S2d). The regression line had an R2 (coefficient of determination) of 0.89, and the volume density of glial cells (g_{vd}) was 55,000 glia/mm³ (95% CI: 24,000–99,000). With the third methodology, we directly estimated the average glial volume density from our measurements of cortical columns across the six species and found glial density to be $44,249 \pm 2,140$ glia/mm³ (mean \pm sem, Table S5), which is not significantly different from the estimates obtained from Fig. 3c. Thus, for each glial cell added to the piriform cortex, neuropil volume increased by 0.022 nL (1/volume density).

As described above, glial volume density calculations using different methodologies were not significantly different from each other. Therefore, for brain regions where we did not have volume estimates, such as PPCx that we describe next, we used these

We distinguish APCx and PPCx measurements for three reasons. First, unlike APCx, PPCx is marked by the absence of the lateral olfactory tract (LOT, which contains olfactory bulb nerve fibers to PCx), a lower neuronal density (29), significantly less input from the olfactory bulb, and more associative input (26). Second, PPCx contains surface-associated astrocytes (SAAs), which are unique to this brain region with their direct apposition to the cortical surface and large-caliber processes that descend into layer 1 (47). Third, functional studies in humans and rodents have suggested that PPCx function differs from that of APCx, mirroring their morphological differences (29, 48-50). In humans (51), while APCx ensembles encoded odor identity, PPCx encoded odor quality or categories, e.g. showing similar response patterns for lemon and lime that can be categorized as citrus fruits. A more recent study showed that PPCx neurons are particularly adept at encoding the differences between odors that are associated with a learning task versus those that are not (52). We, therefore, asked whether, despite the regional proximity of APCx and PPCx, their glial volume densities differ, reflecting functional differences.

Glial volume densities were lower in PPCx compared to APCx (Fig. S3c vs. Fig. 3c). As Fig. S3 shows, the width of the PPCx increases with increasing brain size, and so does the number of glia under a mm². We obtained volume density by normalizing surface area density to PPCx width and from direct volume density

measurements (27,000 glia/mm³, Fig. S3d, 95% CI: 22,522-31,180). The lower density of glia in PPCx compared to APCx mirrors the lower density of neurons in PPCx, the lower number of olfactory bulb inputs, and fewer synapses in layer 1. Thus, the concomitant decrease in glial density with neuronal density and number of synapses suggests glial organization is an additional criterion underlying morphological and functional differences between the two PCx regions.

Glial volume density in the entorhinal cortex remains constant with increasing brain sizes

Next, we investigated if the conservation of glial volume density extended to an architecturally and functionally distinct region: the entorhinal cortex (ECx, Fig. S8a shows a representative section), a multimodal circuit that processes inputs from topographic (e.g. visual) and distributed (e.g. olfactory) circuits. ECx also interacts with the hippocampus (28) and is integral to spatial navigation (27). In this sense, it differs from many of the neocortical regions examined in earlier studies and from the anterior and posterior segments of the piriform cortex, as these regions are primarily sensory regions in which sensory input from peripheral organs (e.g. nose and eyes) is processed.

As Fig. 4a-c shows, ECx volumes and glia numbers increase proportionally across species. Glia occupy a constant fraction of volume in the entorhinal cortex (Fig. 4c) described by the relation, $N_G = 11,000*V_{ECx}$ (R² = 0.969, 95% CI: 7,490–12,570; glial density = 11,000 glia/mm³). Taken together, these data suggest that, for any given region, the number of glia per unit volume remains constant even as brain size changes. Notably, our data also show that the volume density of glia is distinct for APCx, PPCx, and ECx (Fig. S4d), with CI for glial volume densities that do not overlap.

The number of glia per neuron increases with bigger brains in the paleocortex and neocortex

A previous study of the somatosensory, motor, parietal, and temporal regions of the neocortex showed that while neuronal volume densities decrease with bigger brains, glial volume densities remain constant, implying that glia to neuron ratios increase (9). To test if this trend might be general, we estimated glia-neuron ratios (GNRs) and their relation to brain size in brain regions besides the neocortex. In the piriform cortex, glia-neuron ratios increase with brain size, best described by a power-law equation: glia/neurons = $0.7*V_{brain}^{1/4}$ (Fig. 5a), where V_{brain} is brain volume. The neuron data in Fig. 5a are from a previous study (7), while the glia data are from this study. For the piriform alone we had volume estimates measured by the same lab (7), and we found that GNRs increased even faster with piriform size (Fig. S4i, glia/neurons = $0.29*V_{APCx}^{0.5}$). For other regions, however, we did not have volumes from the same lab, so we compared GNRs with brain volume as previously done (10).

In a power-law relationship, the dependent variable y is related to the independent variable x according to the equation $y = ax^b$, where a and b are constants. b is called the scaling exponent and, when positive, determines how fast y grows with respect to x (with negative b's capture how fast y reduces with x; and when b = 1, y's growth is proportional to x).

We examined other architecturally and functionally different regions, to test if such power-laws are observed across the brain. In a previous study, Sherwood et al. (10) reported an increase in glia-neuron ratios with brain size in the prefrontal cortex of primates. Remarkably, when we replotted their data (Fig. 5b), we found that, here, too, glia-neuron ratios increased with brain

size according to a power-law: glia/neurons =0.3* $V_{\textit{brain}}^{1/4}$, where V_{brain} is the brain volume. Interestingly, a 1/4 power-law relationship between glia-neuron ratios and brain volume was also observed in the cerebellum for the ratio of glia to Purkinje cells: glia/neurons =8.75 $*V_{brain}^{1/4}$ (Fig. S4c, data from Ref. (25)). Glia were measured along the extent of the Purkinje cell, which includes the Purkinje layer and most of the molecular layer. The brain volumes in this plot, as well as in Fig. 5a, were taken from Haug (53), and, for the sake of consistency, we only considered glia/neuron ratios of animals whose brain volumes were included in the Haug study. In summary, GNRs scale with brain size similarly in APCx, prefrontal cortex, and the cerebellum.

The conserved GNRs in PCx, PFC, and cerebellum led us to wonder if this might extend to the neocortex as a whole. We examined the literature (53-55) and found glia to neuron ratios in six mammals, including humans, for the whole neocortex (Fig. 5c). Here, too, as brain volume increased, so did the number of glia per neuron according to a power-law: glia/neurons = $0.34*V_{brain}^{1/4}$, suggesting that the scaling of glia to neuron ratios might be conserved across regions and species.

Explanation for GNR power-laws in neocortex

Why would GNR follow a 1/4 power law? To answer this question, we examined data from the neocortex collected in two earlier studies (9, 35). Carlo and Stevens showed two principles of conservation in mammalian neocortices: glial volume densities are the same (q_{vd} : 21,000 glia/mm³) across species, and neuronal surface area densities (number of neurons under a mm² of cortical surface) are the same ($n_{\rm sad}$: 100,000/mm²). From these two findings, we can express the number of glia and neurons under 1 mm² of cortical surface as glia = volume* $g_{vd} = g_{vd}*1*T_{NCx} = 21,000T_{NCx}$, and neurons = $n_{\text{sad}}*surface$ area = $n_{\text{sad}}*1$ = 100,000, where T_{NCx} is the thickness of the neocortex. Furthermore, the thickness, T_{NCx} , (examined in Refs. (9, 35)) and Fig. 5d, covering rodents, carnivores, primates, and insectivores) can be expressed as a function of brain weight (W_{brain}) by the equation, $T_{NCx} = W_{brain}^{1/4}$. Thus, GNR is given by

GNR =
$$\frac{\text{glia}}{\text{neurons}} = \frac{21,000 * W_{brain}^{1/4}}{100,000} = 0.21 W_{brain}^{1/4}$$
. (1)

The analysis shows that the GNR power-law in the neocortex arises because while glial number depends on volume, neuronal number depends on surface area. The ratio of glia to neurons is equivalent to volume to surface area, which is actually cortical thickness, and cortical thickness is related to brain volume by a 1/4 power-law (Fig. 5d). Interestingly, when we examined data available from studies (56) that used a different technique for counting, the isotropic fractionator, the same 1/4 power-law (Fig. S4g, h) was observed. Collectively, these results, which show glia-neuron ratios scaling with brain volume according to a 1/4 power law in diverse regions suggest a feature of brain organization.

Humans and primates have more glia but a similar glial volume density to mice

Previous reports have pointed out that humans might have a higher number of glial cells than other species (57). To test if this might be true, we estimated the number of glia in the anterior piriform cortex of humans. Similar to mice, we estimated the total number of glia using Nissl stains, and numbers of individual glial cell types using DAB staining (astrocytes, microglia, and oligodendrocytes: Figs. 6 and S9) and IF staining (astrocytes alone Fig. S7g, h).

The total number of glia under a square mm of human anterior piriform cortex (APCx) was 46,083 (Fig. 6) with Nissl stains. The surface area of the human APCx was 32.4 mm² leading to around 1.5 million glia in the human APCx. By comparison, the total number of glia in the mouse APCx was 80,000: an order of magnitude lower than humans. The greater number of glia in humans results from the human PCx being much larger by surface area and thickness. This is reflected in human PCx having a higher surface density of glia than mice (46,000 vs. 20,000) or other species with larger brains such as cats (37,000).

Interestingly, the volume density of glia in the human APCx was 42,000 glia/mm³, which is consistent with the volume density of glia in other species (43,000 glia/mm³). Figure 6f shows that the human APCx glial density (in red) falls on the same regression line as other species (replotted Fig. 3c to include humans).

Glial density differences across layers in human PCx mirrored those of mouse PCx. In mice and humans (Figs. 2 and S9g), layer 1 had significantly more glia than other layers, and cell-dense layer 2 had the fewest glia. An in-depth analysis of individual glial cell types shows that, in both species, most of the astrocytes (Figs. 2b and 6b) were in layer 1 (57% in mice, 41% in humans) followed by layer 3 (26% in mice, 35% in humans), and layer 2 (17% in mice, 24% in humans). Microglia (Figs. 2a and 6a) were slightly different with both layers 2 and 3 containing around 30%, with the rest (40%) in layer 1. We left oligodendrocytes out of this analysis as their staining was noticeably lighter (similar to mice, see Fig. S9b for an example). Thus, overall glia, astrocyte and microglia (spatial) distributions were broadly similar in mice and humans, suggesting that glia as a whole might share similarities in organization across species.

The APCx glial distributions in humans and mice were reflected in the distributions of glial cell types (astrocytes and oligodendrocytes) in another primate, the marmoset, in two ways. First, overall glial volume density in marmoset APCx was similar (Fig. 6e). Second, the distribution of astrocytes was similar to humans (compare Figure 6d for humans and Fig. 6e for marmosets), and the distribution of astrocytes and oligodendrocytes was similar to mice (Fig. 2). Interestingly, GFAP staining highlighted interlaminar astrocytes and their processes just below the pial surface (Figs. 1, S7, and 6c) in marmosets and humans but showed their absence in mouse APCx. GFAP staining was stronger in superficial layers and weaker in deeper layers for both species (Fig. S6g, h; lower counts for GFAP+ cells in deeper layers compared to SOX9+ cells, Fig. S9i). Note that in order to make comparisons of overall glial densities, since we did not measure microglia in marmosets, we assumed similar microglial densities for primates in Fig. S7f.

To test if the spatial distribution patterns of glia from mice and humans are recapitulated in other species, we examined glia in each of the APCx layers. Just like in mice and humans, the highest number of glia were found in layer 1 and the lowest in layer 2 (Fig. S5c). We further examined the dataset to test if glial volume densities were different between the layers. As shown in Fig. S5d, glial volume densities are highest in layer 1 followed by layer 3 and layer 2, and the difference between layers 1 and 2 is significant. Thus, glial distributions across layers are likely preserved in mammals. Notably, the distributions of neurons and synapses, too, vary, across layers (26, 29). Layer 1 has the lowest neuronal density and highest synaptic density (29, 58) while layer 2 has the highest neuronal density, suggesting that differences in glia spatial distributions may be a reflection of the different synaptic, neuronal, and neuronal component distributions in each layer (45, 49).

Glial cell type compositions are preserved across species but differ between circuits

As Figs. 3, 4, S3, and S7 show, each region has its own unique glial volume density (Fig. S4d), demonstrating a way to distinguish different circuits (regions) based on morphological characteristics, e.g. glia densities. Figures 2, 6, and S7 further show that even glial cell compositions (i.e. the proportions of glial cell types) of a region might be preserved across species, suggesting another feature of glial organization. To test this hypothesis, we examined snRNA-seq datasets (36–38) (see Materials and methods for details of datasets and analysis) that identified cell type compositions within multiple regions across primate brains, including humans, and tested if glial compositions were (a) similar within a region across species, while (b) differing from other regions in the brain.

In interpreting snRNA-seq datasets, two caveats must be kept in mind. First, experimenter-related variability might arise from researchers dissecting slightly different portions of a given brain region or using different platforms or procedures (37, 38). Second, cell types may be differentially retained or lost during dissociation and nuclear extraction, leading to discrepancies between observed and actual counts. When the comparative datasets, however, are generated by the same lab using consistent protocols, such variability is likely to be minimized and affect cell types similarly across species. The proportions of cell types, rather than absolute numbers, remain meaningful, and conservation despite these sources of variation is itself informative.

Glial cell type composition—ratios of astrocytes, microglia, and oligodendrocytes—is the same across five species of primates that include chimp, gorilla, marmosets, rhesus macaques, and humans. Figure 7a shows the results of analyzing a dataset that examined the cell type composition in the middle temporal gyrus (MTG) of primate brains including humans (36). The MTG is a part of the neocortex in the temporal lobe and has been implicated in diverse functions such as processing of word meanings and gestures (59, 60). They performed snRNA-seq experiments on around 250,000 cells from these species and assigned them to individual cell types like neurons or nonneuronal cells, specifically, astrocytes, microglia, oligodendrocyte-precursor cells or OPCs, and oligodendrocytes. Although including OPCs and oligodendrocytes as separate categories provides a more fine-grained marker, we combined both into a single category to be consistent with our previous findings of three classes in mice and humans. Note that our results do not change if we designate OPCs as a separate category (Fig. S6d). We took this population of nonneuronal cells and computed the relative fraction of these three cell types, i.e. fraction of each population as part of the whole. As Fig. 7a shows, the proportion of astrocytes, microglia, and oligodendrocytes is the same across primates whose brain sizes change over 2 orders of magnitude from marmosets (9.4 g) to humans (1,300 g) (53).

Two concurrent snRNA-seq studies show results consistent with MTG findings. One study characterized more than 2 million cells in various regions of the marmoset brain (38) and another similarly characterized 2.5 million cells in the macaque brain (37). Both studies show evidence that glial cell type compositions are similar in a region across species. The same region in marmosets and macaques, despite differences in methodology, have similar proportions of astrocytes, microglia, and oligodendrocytes (Figs. 7c and S6c). The one notable exception is the cerebellum, which seems to have different numbers of astrocytes and oligodendrocytes (Fig. S6c). In both studies, the cerebellum stands out with its distinctive cell composition, with specialized neuronal classes that may be reflected in glial differences. Additionally,

most cerebellar cells (85% in Ref. (37)) are neurons, so glial composition estimates may vary more because of fewer glial cells and sampling and platform differences. Overall, conservation of glial cell type compositions shows evidence for an additional principle of brain organization.

One possibility, from these results is that glial compositions, like glial densities, might be unique to a circuit as each circuit may require glial cell types in different proportions. As shown in Fig. 7b, the glial cell composition differs from region to region. For instance, compare the third row from the top (cortex) and the second row from the bottom (basal ganglia). The cortex contains many more astrocytes than the basal ganglia, marginally fewer microglia, and far fewer oligodendrocytes. This is reflected in the vertical bar plots of Fig. 7c, where glial cell compositions are different between brain regions. The trend remained when we included APCx measurements from humans and mice (Fig. S6e), where each region's glial cell composition is conserved while differing from others.

Thus, glial organization in each region is conserved across species and distinguished from other regions by the unique combination of astrocytes, microglia, and oligodendrocytes within a mm³ (Fig. S6e), likely reflecting the unique computations of each region.

Discussion

We have identified three consistent features of glial organization—in terms of densities and cell compositions—in humans, other primates, carnivores and model organisms such as mice and rats (Figs. 3-7) that may reflect underlying organizing principles. First, glial volume density was conserved within brain regions (across species), while differing across them. This property was observed in five brain regions (Fig. 3c, anterior piriform cortex; Fig. S3c, posterior piriform cortex; Fig. 4c, entorhinal cortex; (9), neocortex; Fig. S4b, cerebellum; Fig. S4d, comparison of all regions) that differ from each other in terms of morphology, connectivity, and function. Second, glial cell type compositions, too, were preserved within regions, while significantly changing across regions in humans, other primates, and mice (Figs. 2, 6, and 7 and summary in Fig. S6e). Third, in the piriform cortex, neocortex (including primate frontal cortex), and the cerebellum, the number of glia per neuron increased with brain volume according to a 1/4 power law (Figs. 5 and S4 and illustration in Fig. 8).

Consistency between individual and overall counts of glia types

We used four methods to quantify glial cells in the brain: Sox9-EGFP mice, DAB stains, IF stains, and Nissl stains. Of the methods, Nissl stained tissue covered the greatest number of species. Notably, the Nissl stained set overlapped with DAB and IF stained sets, and Sox9-EGFP mice, providing a validation of Nissl stained counts. DAB and IF staining were used to quantify the major glial cell types—astrocytes, microglia, and oligodendrocytes—and their densities in the piriform cortex of humans, marmosets, and mice (Figs. 2 and 6). With the Sox9-EGFP mice, we estimated astrocyte/ neuron ratios using GFP to mark astrocytes and NeuN to mark neurons

The counts from the different methods revealed consistent patterns in glial cell-type distributions in at least three ways. First, the astrocyte/neuron ratios measured using Sox9-EGFP and DAB staining were consistent (Fig. S1). Second, the astrocyte/oligodendrocyte ratios with DAB and IF stainings were

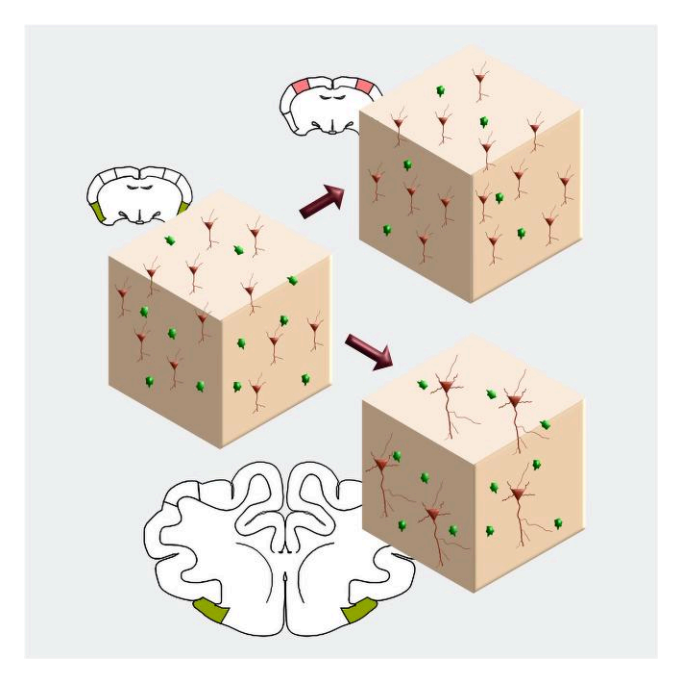


Fig. 8. An illustration of two features of glia organization. First, glial density is conserved within a brain region across species. Compare the piriform cortex in cat (bottom) and mouse (left) in the ventral-lateral region. Even as the piriform and brain sizes change between the two species, the number of glia is conserved within a cube of piriform cortex tissue. Second, the number of neurons is reduced from the mouse to cat, leading to an increase in GNR ratios with an increase in brain size. Notably, the number of glia and neurons change across brain regions: compare the piriform cortex (middle left) and neocortex (top) in mice. Glial densities can, thus, serve as region specific markers. Note that for ease of illustration the coronal section schematics for mouse and cat are not drawn to scale. The cat is drawn at half the actual scale, which means the cat section is actually twice as large as shown in the figure.

similar between humans and mice, and marmosets and mice, respectively (Fig. S7c). As mice had IF and DAB staining, we compared the two stains. IF staining identified a higher number of oligodendrocytes (in layer 3) and subsequently a higher ratio of oligodendrocytes/astrocytes (Fig. S7c). Third, the staining for individual cell-types with DAB and IF, and all glia with Nissl were consistent for humans, marmosets, and mice (Figs. 2, 6, and S7a), and provide strong support for using Nissl stains to estimate glial cell distributions in different brain regions across species. This is perhaps one of the reasons that previous quantitative studies used similar methodologies (9, 25, 39) for cross-species comparisons, which would not have been possible otherwise.

Studies from the literature provide added validation of our glial estimates. They include findings of conserved glial volume densities in the neocortex (parietal, somatosensory, and motor cortices) in mice, rats, cats, and macaques (9); conserved glial volume densities in the neocortex of insectivores (35); and diverse astrocyte densities across regions in the mouse brain correlating with molecular diversity (61). A more recent study (62) examined layer 1 of PFC and found densities of glia and GFAP marked astrocytes to be similar across four species of primates including humans, which had slightly higher densities of astrocytes. Similarly, studies using alternative methods to stereology (56) found GNRs similar to our findings (Fig. S4).

While these cross-validations strengthen our confidence in the findings, similar to snRNA-seq experiments, histology experiments are also subject to experimental variability. Variability can arise from species-specific differences in staining, differences in the staining of different markers for the same kind of cell, and

differences in imaging various types of stains. Despite such variability, consistency across multiple methods and agreement with literature studies suggest the presence of underlying features of organization.

Glial density and composition change across circuits

Two findings show that brain regions can be distinguished based on glial volume density and composition within that region (Figs. S4d and S6e). First, glial densities differ between brain regions while being conserved within a region across species (Figs. 3, 4, S3, and S4d, (63)). Second, glial cell compositions are maintained within a region across species, but, differ between regions (Figs. 7 and S6e; (63)). We note that while our study examined two of the regions covered by the primate snRNA-seq studies of Fig. 7b, (37, 38) also include regions we did not examine, e.g. basal ganglia. Although our data strongly suggest that glial volume densities will also be conserved across these regions, future studies to validate this would be important.

Glial density and composition have the property of a regional marker in the regions and species we examined. A regional marker stays the same in a region across species, but varies between regions. In some cases, e.g. the neocortex and cerebellum, regions have similar densities, but varying glial cell compositions (snRNA-seq experiments) can distinguish the two regions (Fig. S6c, compare CX and CB regions). Put another way, cell composition proportions seem to implement a combinatorial code, wherein the combination of glial cell type proportions can distinguish one region from the next. Notably, neuronal densities (7, 10, 20), which decrease with brain size, cannot serve as regional markers.

Our study provides evidence that glial characteristics change across circuits and may serve as potential indicators of structural differences between circuits. This spatial heterogeneity of glia has also been observed by others (64–67). Since circuits are known to perform different functions, glial organization could potentially correlate with functional differences, but establishing such relationships would require future studies that directly measure both glial features and functional properties within the same circuits. Our findings lay the groundwork for such investigations by demonstrating that glial density and composition provide reliable circuit-specific signatures that are conserved across species.

Our observations raise two questions. First, what factors determine the glial cell composition in a region? Although outside this study's scope, prior work provides clues of how astrocytes, microglia, and oligodendrocytes might be differentially regulated based on function. All circuits have to form, remove or maintain synapses, communicate with other circuits, and clear cell debris (11). It is not surprising that all three glial cell types are present across brain regions (Figs. 7 and S6). There are regions, however, that require more of one class. Oligodendrocytes produce myelin that enables better communication between neurons. In primates, they are highly expressed in the brain stem of macaques and marmosets (Fig. 7b) as well as the corpus callosum of marmosets (Fig. S6): two regions that have a high density of white matter (68). Another example is APCx. We found that layer 3 contains a high number of oligodendrocytes matching higher expressions of NF-160 and SMI-99 in layer 3 (Fig. S8b). The two proteins label axon filaments and myelin.

Similarly, our study found that astrocytes, which are important for synapse function (14, 43), are the most numerous glial cell type in PCx layer 1. PCx layer 1 comprises an all-to-all connection matrix between OB and PCx (7) with a large number of synapses and

is particularly synapse-rich (26, 29, 58). Measurements of glial surface density (Table S1) show that layer 1 of the (69) piriform cortex has a greater number of glial cells and astrocytes (Figs. 2, 5, and S5) across species. It is possible the link between synapse-dense layers of the piriform cortex and higher numbers of glia and astrocytes (70) might be recapitulated in other synapse rich areas of the brain.

Lastly, microglia significantly increase in regions associated with immune responses and inflammation during aging (71); in effect they are better markers for aging than neurons, e.g. in rats, the number of microglia increased (about 16%) in the frontal and parietal regions associated with axon and dendrite degradation (72, 73). Interestingly, microglial densities vary across the brain, unlike earlier reports (74), with the cerebellum having particularly low numbers, while the prefrontal cortex has high numbers (74, 75) (Fig. 7b). Further investigation of correlations between glial cell type changes across regions and factors such as plasticity, synaptic density, and myelination will give us insight into the roles of glial cells in local circuit computations and the overall brain.

Glial cell sampling of space is region dependent

As glial densities differ between regions (Fig. S4d), the regional volume they serve will change, too. Each glial cell in APCx occupies a neuropil volume covering 0.022 nL, which corresponds to a cube with sides of 28 μm. Similarly, glial cells in PPCx, neocortex, and ECx occupy a cube with sides $32 \mu m$, $36-40 \mu m$ (76-78), and 46μ m, respectively.

Two factors could drive density differences across circuits. The first factor is heterogeneity in glial cell-types across the brain (75, 79-84), wherein glial morphologies are conserved within a circuit but vary across them. This could lead them to occupy different amounts of neuropil volume across circuits. For instance, in the mouse, astrocyte densities show abrupt changes at cell borders (61), and their morphologies vary between regions (85) supporting circuit-specificity. In the hippocampus, astrocyte sizes and morphologies even differ between individual layers (86, 87). Similarly, as in our APCx studies, morphological characteristics such as density may vary across layers that perform different functions. These studies link changes in structure (morphology) and function, and suggest one possible source of varying densities across circuits.

Second, changes in glial cell compositions can impact glial volume densities. Glial cell types come in different sizes (77, 88, 89). If the proportion of a particular cell type, e.g. astrocytes, is higher in one region compared to another, the difference in cell sizes would affect how many glial cells can be packed into a given volume, affecting density. Thus, variations in both glial morphologies and glial cell compositions across brain circuits can account for differences in glial densities.

The link between densities and glial compositions also speaks to previous proposals of achieving constant density (21). Three possibilities were suggested: (i) the volume densities of astrocytes, microglia, and oligodendrocytes stay the same, (ii) one of the celltypes predominates so that variations in the other two do not affect overall density, and (iii) reduction in the number of one type is compensated by another. Of the three hypotheses, our data show evidence for the first. Across MTG in primates, various brain regions in marmosets and macaques, and PCx in humans, marmosets, and mice, glial cell compositions are similar within a region. Moreover, the other two possibilities require that glial cell type sizes be similar, which is unlikely (77, 88, 89). Although a mixture of the three mechanisms is also possible, our data present evidence that constant glial volume density in a region arises primarily from conserved glial cell compositions.

Conservation of glial volume density might not be exclusive to the forebrain: a possibility supported by reanalysis of a study of the cerebellum by Friede (25). Friede examined the cerebellum of 18 species including birds, rodents, and mammals, to estimate glial volume density and the number of glia per Purkinje cell. While he examined the entire cerebellar cortex, glial counts are from the Purkinje cell layer, and the portion of the molecular layer that contained Purkinje cell dendrites. The thickness of the molecular layer averaged to 360 μ m (Fig. S9c). Although the author interpreted glial volume densities to be variable between species, we found that densities were normally distributed around a mean of 22,840 glia/mm³ (Fig. S4a, b, c); note that the list does not include five species of nonmammals in which glia densities were intriguingly higher. This value, with an associated SEM of 1,592, likely represents the true density of glia in 13 of the 18 mammalian species studied (Fig. S4a, b, c), corresponding to glia occupying a cube of side $36 \mu m$. Therefore, in the four regions—neocortex, paleocortex, entorhinal cortex, and cerebellum—the inter-glial distance changes, likely reflecting the differing functional demands of each region.

Glia-neuron ratios increase with brain size

Conserved GNRs suggest a strong functional coupling between glia and neurons, which is integral to circuit function (90). We show that GNR increased with brain volumes according to a 1/4 powerlaw in four brain regions: the anterior piriform cortex (Fig. 5a), the prefrontal cortex of primates (Fig. 5b), cerebellum (Fig. S4c), and the cerebral cortex as a whole (Fig. 5c) in mammals (also illustrated in Fig. 8). Interestingly, for the piriform alone, we had measurements of region size from the same lab (important for consistency), and found that GNRs increased even more rapidly (Fig. S4i, 1/2 power-law). This raises the possibility that glia numbers might increase relative to neurons more rapidly than traditionally thought, and a question warranting further exploration.

Higher GNRs in bigger-brained species have led researchers to hypothesize that cognitive abilities improve with higher GNRs (91–93). For instance, it was reported that Brodmann area 39 of Einstein's brain, part of the parietal lobe, had significantly more glia per neuron than eleven other male subjects (57). While GNRs in Brodmann area 39 were higher for Einstein, other factors were not significantly different. When comparing multiple variables, it is possible that one of the variables is statistically significant by chance. To establish the hypothesis, one would need to systematically investigate whether individuals with high cognitive abilities have above average GNRs and vice-versa. These studies could then address whether both characteristics arise from a common root or are causally related.

Why do bigger brains have more glia per neuron? As brain size increases, neuronal and glial functional requirements vary. Glial function, which is mostly local, does not change dramatically. Neurons, however, have to communicate over longer distances, both locally, and long-range to transmit information in a comparable amount of time to smaller brains (1). As a result, axon diameters increase to enable greater conduction velocities (94-97), leading to a greater amount of wire in extracellular space. An example is the 5/4 power-law increase in cortical white matter compared to gray matter across brain sizes (5). Bigger axons also necessitate bigger somas (20, 97). These factors do increase glia sizes though to a much smaller extent.

An assessment of quantitative data for the neocortex shows evidence for this trend. While neurons increase with surface area, glia increase with volume (9, 98). Because cortical thickness (which represents the ratio between volume and surface area)

scales as a 1/4 power-law with brain volume (Fig. 5d), glia increase faster, yielding higher GNRs with bigger brains.

These patterns of glial organization provide yet more evidence that circuits are optimally designed. The widespread conservation of neuronal architectures from flies to mammals separated by 450 million years is strong evidence that evolution has worked out an optimal solution for neuronal machinery. Extra neuronal machinery increases energy usage at the cost of diminishing returns and is not advantageous (99). Conserved glial densities and cell compositions in different regions suggest a similar evolutionary constraint for glia. Glia are just as likely as neurons to be precisely engineered and any additional glial machinery will add to the system's cost without providing any extra benefits, which is a reason for conserved relationships.

Astrocyte heterogeneity

An excellent example of species-specific differences in glial morphologies comes from an in-depth study of astrocytes in mice and humans. It showed human astrocyte somas to be larger, having larger and more numerous processes (82). Similar findings in ferrets (100) and even nonhuman primates (macaques and chimp (62)) suggest a possible trend that astrocytes increase in size with larger species. These morphological differences are reflected in functional differences, wherein calcium propagation is faster in human astrocytes (82) and transplanted human astrocytes improve circuit function (101).

Our examination of astrocytes in PCx of humans, marmosets, and mice is consistent with these findings. Astrocyte volume densities were similar in these species (Figs. 2 and 6). With constant densities, astrocyte cell bodies must be similar distances apart, suggesting that if human astrocyte territories are larger, there must be increasing overlap in the territories of neighboring astrocytes. This is, indeed, true for ferrets and humans compared to mice (82, 100). Thus, studies ranging from those showing astrocytes tiling a region and apportioning equal territories in the mouse hippocampus (76, 102) to ones showing increasing overlap in bigger species (82, 100) are consistent with our findings of conserved volume densities.

Conclusions

Drawing on approaches used in neuronal scaling (3, 5, 7, 10, 103), we investigated glial scaling to gain high-level insights into the role of glia. We identified conserved features of glial organization in mammals (including humans), wherein densities and compositions are maintained within a region, yet vary across regions. Moreover, glia and neurons are tightly coupled, suggesting that these glial organizational features have implications for human neurophysiology and disease.

While most studies examining brain diseases and disorders have focused on the breakdown of neuronal machinery, far fewer have examined the consequences of glial dysfunction. Yet, studies of glia in brain disorders, including Alzheimer's disease (104, 105), underscore their importance in neurodegenerative diseases. Our work calls for a holistic view that incorporates neurons and glia, and their interactions, as drivers of disease mechanisms.

Acknowledgments

We thank Chuck Stevens for providing resources and guidance. We thank Scott Magness for providing us with Sox9-EGFP mice; Margarita Behrens for lab support, Nicola Allen and Ashley Brandebura for technical and reagent help for the DAB experiments, Gerald Pao, Junko Ogawa, and Shrek Chalasani for help with mouse OLIG2 experiments, and we are especially grateful to Yukiko Goda, Eiman Azim, and Vasileios Glykos for help with the IF experiments, Phong Ngyuyen for help and advise with both experiments, Jorge Aldana for computational assistance, and J. Dennis Bender for support. We also appreciate Nicolla Allen, Sinda Fekir, and the reviewers for their valuable feedback. We would also like to thank the Theoretical Science Visiting Fellowship at OIST for a fellowship and support for SS.

Supplementary Material

Supplementary material is available at PNAS Nexus online.

Funding

This research was funded in part by the Kavli Institute at UCSD, National Institutes of Health DC017695, and National Science Foundation Next Generation Networks for Neuroscience 2 2014862.

Author Contributions

A.P.-D.: formal analysis; investigation; methodology; writing-original draft; writing-review and editing. K.B.: data curation; investigation; methodology. T.S.: resources; funding acquisition; project administration; writing-review and editing. S.S.: conceptualization; data curation; software; formal analysis; supervision; funding acquisition; investigation; methodology; writingoriginal draft; project administration; writing-review and editing.

Preprints

This manuscript was posted on a preprint: https://doi.org/10. 1101/449421.

Data Availability

The data for the plots in the main article are at DOI: 10.5281/ zenodo.17191216.

References

- Buzsáki G, Logothetis N, Singer W. 2013. Scaling brain size, keeping timing: evolutionary preservation of brain rhythms. Neuron. 80(3):751-764.
- Cuntz H, Mathy A, Hausser M. 2012. A scaling law derived from optimal dendritic wiring. Proc Natl Acad Sci. 109(27):11014-11018.
- Finlay BL, Darlington RB. 1995. Linked regularities in the development and evolution of mammalian brains. Science. 268(5217):
- Stevens CF. 2001. An evolutionary scaling law for the primate visual system and its basis in cortical function. Nature. 411(6834): 193-195.
- Zhang K, Sejnowski TJ. 2000. A universal scaling law between gray matter and white matter of cerebral cortex. Proc Natl Acad Sci U S A. 97(10):5621-5626.
- Srinivasan S, Carlo CN, Stevens CF. 2015. Predicting visual acuity from the structure of visual cortex. Proc Natl Acad Sci U S A. 112(25):7815-7820.
- Srinivasan S, Stevens CF. 2019. Scaling principles of distributed circuits. Curr Biol. 29(15):2533-2540.

- Von Bartheld CS, Bahney J, Herculano-Houzel S. 2016. The search for true numbers of neurons and glial cells in the human brain: a review of 150 years of cell counting. J Comp Neurol. 524(18):3865-3895.
- Carlo CN, Stevens CF. 2013. Structural uniformity of neocortex, revisited. Proc Natl Acad Sci U S A. 110(4):1488-93.
- 10 Sherwood CC, et al. 2006. Evolution of increased glia-neuron ratios in the human frontal cortex. Proc Natl Acad Sci USA. 103(37): 13606-13611
- Allen NJ, Lyons DA. 2018. Glia as architects of central nervous system formation and function. Science. 362(6411):181-185.
- Mu Y, et al. 2019. Glia accumulate evidence that actions are futile and suppress unsuccessful behavior. Cell. 178(1):27-43.
- 13 Pinto-Duarte A, Roberts AJ, Ouyang K, Sejnowski TJ. 2019. Impairments in remote memory caused by the lack of type 2 ip3 receptors. Glia. 67(10):1976-1989.
- Saint-Martin M, Goda Y. 2023. Astrocyte-synapse interactions and cell adhesion molecules. FEBS J. 290(14):3512-3526.
- Santello M, Toni N, Volterra A. 2019. Astrocyte function from information processing to cognition and cognitive impairment. Nat Neurosci. 22(2):154-166.
- Baldwin KT, Murai KK, Khakh BS. 2024. Astrocyte morphology. Trends Cell Biol. 34(7):547-565.
- Wolf SA, Boddeke H, Kettenmann H. 2017. Microglia in physiology and disease. Annu Rev Physiol. 79(1):619-643.
- Bradl M, Lassmann H. 2010. Oligodendrocytes: biology and pathology. Acta Neuropathol. 119(1):37-53.
- Kuhn S, Gritti L, Crooks D, Dombrowski Y. 2019. Oligodendrocytes in development, myelin generation and beyond. Cells. 8(11):1424.
- Herculano-Houzel S. 2014. The glia/neuron ratio: how it varies uniformly across brain structures and species and what that means for brain physiology and evolution. Glia. 62(9):1377-1391.
- Herculano-Houzel S, Dos Santos SE. 2018. You do not mess with the glia. Neuroglia. 1(1):193-219.
- 22 Siletti K, et al. 2023. Transcriptomic diversity of cell types across the adult human brain. Science. 382(6667):eadd7046.
- Andersen BB, Gundersen HJG, Pakkenberg B. 2003. Aging of the human cerebellum: a stereological study. J Comp Neurol. 466(3):
- 24 Andersen BB, Korbo L, Pakkenberg B. 1992. A quantitative study of the human cerebellum with unbiased stereological techniques. J Comp Neurol. 326(4):549-560.
- Friede RL. 1963. The relationship of body size, nerve cell size, axon length, and glial density in the cerebellum. Proc Natl Acad Sci U S A. 49(2):187-193.
- 26 Neville KR, Haberly LB. 2004. Olfactory cortex. Synaptic Organ Brain. 5:415-454.
- Fyhn M, Molden S, Witter MP, Moser EI, Moser M-B. 2004. Spatial representation in the entorhinal cortex. Science. 305(5688):
- Witter MP, Doan TP, Jacobsen B, Nilssen ES, Ohara S. 2017. Architecture of the entorhinal cortex a review of entorhinal anatomy in rodents with some comparative notes. Front Syst
- Srinivasan S, Stevens CF. 2018. The distributed circuit within the piriform cortex makes odor discrimination robust. J Comp Neurol. 526(17):2725-2743.
- Garcia-Cabezas MA, John YJ, Barbas H, Zikopoulos B. 2016. Distinction of neurons, glia and endothelial cells in the cerebral cortex: an algorithm based on cytological features. Front Neuroanat. 10:107.

- 31 Ding S-L, et al. 2016. Comprehensive cellular-resolution atlas of the adult human brain. J Comp Neurol. 524(16):3127-3481.
- Mai JK, Majtanik M, Paxinos G. Atlas of the human brain. Academic Press, 2015.
- 33 Paxinos G, Franklin KBJ. The mouse brain in stereotaxic coordinates. Gulf Professional Publishing, 2004.
- Snider RS, Niemer WT. Stereotaxic atlas of the cat brain. University of Chicago Press, 1961.
- Stolzenburg J-U, Reichenbach A, Neumann M. 1989. Size and density of glial and neuronal cells within the cerebral neocortex of various insectivorian species. Glia. 2(2):78-84.
- Jorstad NL, et al. 2023. Transcriptomic cytoarchitecture reveals principles of human neocortex organization. Science. 382(6667): eadf6812.
- Chiou KL, et al. 2023. A single-cell multi-omic atlas spanning the adult rhesus macaque brain. Sci Adv. 9(41):eadh1914.
- Krienen FM. et al. 2023. A marmoset brain cell census reveals regional specialization of cellular identities. Sci Adv. 9(41): eadk3986.
- Sun W, et al. 2017. Sox9 is an astrocyte-specific nuclear marker in the adult brain outside the neurogenic regions. J Neurosci. 37(17):4493-4507.
- Eng LF, Vanderhaeghen JJ, Bignami A, Gerstl B. 1971. An acidic protein isolated from fibrous astrocytes. Brain Res. 28(2):
- 41 Matias I, Morgado J, Gomes FCA. 2019. Astrocyte heterogeneity: impact to brain aging and disease. Front Aging Neurosci. 11:59.
- Falcone C, et al. 2021. Cortical interlaminar astrocytes are generated prenatally, mature postnatally, and express unique markers in human and nonhuman primates. Cereb Cortex. 31(1):379-395.
- Allen NJ, Eroglu C. 2017. Cell biology of astrocyte-synapse interactions. Neuron. 96(3):697-708.
- Verkhratsky A, Nedergaard M, Hertz L. 2015. Why are astrocytes important? Neurochem Res. 40(2):389-401.
- Bekkers JM, Suzuki N. 2013. Neurons and circuits for odor processing in the piriform cortex. Trends Neurosci. 36(7):429-38.
- Suzuki N, Bekkers JM. 2011. Two layers of synaptic processing by principal neurons in piriform cortex. J Neurosci. 31(6): 2156-66.
- Feig SL, Haberly LB. 2011. Surface-associated astrocytes, not endfeet, form the glia limitans in posterior piriform cortex and have a spatially distributed, not a domain, organization. J Comp Neurol. 519(10):1952-1969.
- Calu DJ, Roesch MR, Stalnaker TA, Schoenbaum G. 2007. Associative encoding in posterior piriform cortex during odor discrimination and reversal learning. Cereb Cortex. 17(6): 1342-1349.
- Haberly LB. 2001. Parallel-distributed processing in olfactory cortex: new insights from morphological and physiological analysis of neuronal circuitry. Chem Senses. 26(5):551-576.
- Hagiwara A, Pal SK, Sato TF, Wienisch M, Murthy VN. 2012. Optophysiological analysis of associational circuits in the olfactory cortex. Front Neural Circuits. 6:18.
- 51 Howard JD, Plailly J, Grueschow M, Haynes J-D, Gottfried JA. 2009. Odor quality coding and categorization in human posterior piriform cortex. Nat Neurosci. 12(7):932-938.
- Berners-Lee A, Shtrahman E, Grimaud J, Murthy VN. 2023. Experience-dependent evolution of odor mixture representations in piriform cortex. PLoS Biol. 21(4):e3002086.
- Haug H. 1987. Brain sizes, surfaces, and neuronal sizes of the cortex cerebri: a stereological investigation of man and his variability and a comparison with some mammals (primates,

- whales, marsupials, insectivores, and one elephant). Am J Anat. 180(2):126-42.
- Christensen JR, et al. 2007. Neocortical and hippocampal neuron and glial cell numbers in the rhesus monkey. Anat Rec (Hoboken).
- Verkhratsky A, Butt AM. 2018. The history of the decline and fall of the glial numbers legend. Neuroglia. 1(1):188-192.
- 56 Herculano-Houzel S, Catania K, Manger PR, Kaas JH. 2015. Mammalian brains are made of these: a dataset of the numbers and densities of neuronal and nonneuronal cells in the brain of glires, primates, scandentia, eulipotyphlans, afrotherians and artiodactyls, and their relationship with body mass. Brain Behav Evol. 86(3-4):145-163.
- Diamond MC, Scheibel AB, Murphy Jr GM, Harvey T. 1985. On the brain of a scientist: Albert Einstein. Exp Neurol. 88(1):
- Schikorski T, Stevens CF. 1999. Quantitative fine-structural analysis of olfactory cortical synapses. Proc Natl Acad Sci U S A. 96(7):4107-12.
- Geschwind N. 1970. The organization of language and the brain: language disorders after brain damage help in elucidating the neural basis of verbal behavior. Science. 170(3961):940-944.
- Papeo L, Agostini B, Lingnau A. 2019. The large-scale organization of gestures and words in the middle temporal gyrus. J Neurosci. 39(30):5966-5974.
- Endo F, et al. 2022. Molecular basis of astrocyte diversity and morphology across the CNS in health and disease. Science. 378(6619):eadc9020.
- Munger EL, et al. 2022. Comparative analysis of astrocytes in the prefrontal cortex of primates: insights into the evolution of human brain energetics. J Comp Neurol. 530(18):3106-3125.
- Keller D, Erø C, Markram H. 2018. Cell densities in the mouse brain: a systematic review. Front Neuroanat. 12:83.
- Bocchi R, et al. 2025. Astrocyte heterogeneity reveals regionspecific astrogenesis in the white matter. Nat Neurosci. 28:1-13.
- Chai H, et al. 2017. Neural circuit-specialized astrocytes: transcriptomic, proteomic, morphological, and functional evidence. Neuron. 95(3):531-549.
- Seeker LA, et al. 2023. Brain matters: unveiling the distinct contributions of region, age, and sex to glia diversity and CNS function. Acta Neuropathol Commun. 11(1):84.
- Sun J, et al. 2022. Heterogeneity and molecular markers for CNS glial cells revealed by single-cell transcriptomics. Cell Mol Neurobiol. 42(8):2629-2642.
- Buyanova IS, Arsalidou M. 2021. Cerebral white matter myelination and relations to age, gender, and cognition: a selective review. Front Hum Neurosci. 15:662031.
- Eroglu C, Barres BA. 2010. Regulation of synaptic connectivity by glia. Nature. 468(7321):223-231.
- 70 Faraguna U, Nelson A, Vyazovskiy VV, Cirelli C, Tononi G. 2010. Unilateral cortical spreading depression affects sleep need and induces molecular and electrophysiological signs of synaptic potentiation in vivo. Cereb Cortex. 20(12):2939-2947.
- Soreq L, et al. 2017. Major shifts in glial regional identity are a transcriptional hallmark of human brain aging. Cell Rep. 18(2): 557-570.
- Peinado MA, Martinez M, Pedrosa JA, Quesada A, Peinado JM. 1993. Quantitative morphological changes in neurons and glia in the frontal lobe of the aging rat. Anat Rec. 237(1):104-108.
- Peinado MA, et al. 1997. Light microscopic quantification of morphological changes during aging in neurons and glia of the rat parietal cortex. Anat Rec. 247(3):420-425.

- 74 Dos Santos SE, et al. 2020. Similar microglial cell densities across brain structures and mammalian species: implications for brain tissue function. *J Neurosci.* 40(24):4622–4643.
- 75 Tan Y-L, Yuan Y, Tian L. 2020. Microglial regional heterogeneity and its role in the brain. *Mol Psychiatry*. 25(2):351–367.
- 76 Halassa MM, Fellin T, Takano H, Dong J-H, Haydon PG. 2007. Synaptic islands defined by the territory of a single astrocyte. J Neurosci. 27(24):6473–6477.
- 77 Oberheim NA, Goldman SA, Nedergaard M. 2012. Heterogeneity of astrocytic form and function. *Methods Mol Biol.* 814:23–45.
- 78 Ogata K, Kosaka T. 2002. Structural and quantitative analysis of astrocytes in the mouse hippocampus. Neuroscience. 113(1): 221–233.
- 79 Emsley JG, Macklis JD. 2006. Astroglial heterogeneity closely reflects the neuronal-defined anatomy of the adult murine CNS. Neuron Glia Biol. 2(3):175–186.
- 80 Falcone C. 2022. Evolution of astrocytes: from invertebrates to vertebrates. Front Cell Dev Biol. 10:931311.
- 81 Foerster S, Hill MFE, Franklin RJM. 2019. Diversity in the oligodendrocyte lineage: plasticity or heterogeneity? Glia. 67(10): 1797–1805.
- 82 Oberheim NA, et al. 2009. Uniquely hominid features of adult human astrocytes. J Neurosci. 29(10):3276–3287.
- 83 Osanai Y, Yamazaki R, Shinohara Y, Ohno N. 2022. Heterogeneity and regulation of oligodendrocyte morphology. Front Cell Dev Biol. 10:1030486.
- 84 Haim LB, Rowitch DH. 2017. Functional diversity of astrocytes in neural circuit regulation. *Nat Rev Neurosci.* 18(1):31–41.
- 85 Marini M, et al. 2025. Supervised and unsupervised learning reveal heroin-induced impairments in astrocyte structural plasticity. Sci Adv. 11(18):eads6841.
- 86 Karpf J, et al. 2022. Dentate gyrus astrocytes exhibit layerspecific molecular, morphological and physiological features. Nat Neurosci. 25(12):1626–1638.
- 87 Viana JF, et al. 2023. Astrocyte structural heterogeneity in the mouse hippocampus. Glia. 71(7):1667–1682.
- 88 Davis BM, Salinas-Navarro M, Francesca Cordeiro M, Moons L, De Groef L. 2017. Characterizing microglia activation: a spatial statistics approach to maximize information extraction. Sci Rep. 7(1):1576.

- 89 Rajkowska G, Selemon LD, Goldman-Rakic PS. 1998. Neuronal and glial somal size in the prefrontal cortex: a postmortem morphometric study of schizophrenia and Huntington disease. *Arch Gen* Psychiatry. 55(3):215–224.
- 90 Sun W, et al. 2024. Spatial transcriptomics reveal neuron-astrocyte synergy in long-term memory. Nature. 627(8003):374–381.
- P1 Fields RD. 2004. The other half of the brain. Sci Am. 290(4):54–61.
- 92 Franklin RJM, Bussey TJ. 2013. Do your glial cells make you clever? Cell Stem Cell. 12(3):265–266.
- 93 Spitzer S, Agathou S, Karadottir RT. 2013. Clever glia. Stem Cell Res Ther. 4(4):1–2.
- 94 Hursh JB. 1939. Conduction velocity and diameter of nerve fibers. Am J Physiol-Leg Content. 127(1):131–139.
- 95 Innocenti GM. 2011. Development and evolution: two determinants of cortical connectivity. *Prog Brain Res.* 189:65–75.
- 96 Ritchie JM. 1982. On the relation between fibre diameter and conduction velocity in myelinated nerve fibres. *Proc R Soc Lond B Biol Sci.* 217(1206):29–35.
- 97 Sakai H, Woody CD. 1988. Relationships between axonal diameter, soma size, and axonal conduction velocity of hrp-filled, pyramidal tract cells of awake cats. *Brain Res.* 460(1):1–7.
- 98 Rockel AJ, Hiorns RW, Powell TP. 1980. The basic uniformity in structure of the neocortex. *Brain*. 103(2):221–244.
- 99 Sterling P, Laughlin S. Principles of neural design. MIT Press, 2015.
- 100 Lopez-Hidalgo M, Hoover WB, Schummers J. 2016. Spatial organization of astrocytes in ferret visual cortex. *J Comp Neurol*. 524(17):3561–3576.
- 101 Han X, et al. 2013. Forebrain engraftment by human glial progenitor cells enhances synaptic plasticity and learning in adult mice. Cell Stem Cell. 12(3):342–353.
- 102 Bushong EA, Martone ME, Jones YZ, Ellisman MH. 2002. Protoplasmic astrocytes in CA1 stratum radiatum occupy separate anatomical domains. *J Neurosci.* 22(1):183–192.
- 103 Herculano-Houzel S. 2010. Coordinated scaling of cortical and cerebellar numbers of neurons. Front Neuroanat. 4:12.
- 104 Derevyanko A, Tao T, Allen NJ. 2025. Common alterations to astrocytes across neurodegenerative disorders. Curr Opin Neurobiol. 90:102970.
- 105 Rao C, Semrau S, Fossati V. 2025. Decoding microglial functions in Alzheimer's disease: insights from human models. Trends Immunol. 46(4):310–323.